Surface structure of alanine on Cu(110) via grazing scattering of fast atoms and molecules

J. Seifert,* M. Busch, E. Meyer, and H. Winter
Institut für Physik, Humboldt-Universität zu Berlin, Newtonstraße 15, D-12489 Berlin, Germany
(Received 14 November 2013; published 7 February 2014)

We have studied structures of the chiral amino acid alanine adsorbed on Cu(110) via low-energy electron diffraction (LEED) as well as scattering of fast light atoms and molecules. The adsorption process was controlled *in situ* by the intensity of specularly reflected 2-keV He atoms. For projectile energies less than 1 keV, we applied the method of fast atom diffraction for studies on the structure of adsorbed alanine molecules on an atomically flat Cu(110) surface with focus on a $p(3 \times 2)$ adsorbate phase. The results are consistent with LEED and explain distortions in LEED patterns via an elongated surface unit cell with incommensurate $c(3.16 \times 2)$ symmetry of parts of the adsorbate. From triangulation using fast atoms via the azimuthal rotation of the target surface, the positions of protruding methyl groups are derived.

DOI: 10.1103/PhysRevB.89.075404 PACS number(s): 34.35.+a, 68.55.am, 68.49.−h, 68.43.Fg

I. INTRODUCTION

Studies on the nanoscale and control of supramolecular assembly of organic molecules on metal surfaces are prerequisites for the realization and detailed understanding of nanotechnological applications in sensors and molecular electronics, as well as heterogenous catalysis [1,2]. Of special interest are chiral molecules, which are incongruent with their mirror image. Chiral molecules of living organisms appear predominantly in one enantiomeric form and possess different biological activities. Thus the study of chirality of molecules at surfaces has considerable relevance for pharmaceutical and agrochemical applications with the prospect of enantioselective heterogenous catalysis [3]. In this respect the smallest (intrinsically) chiral amino acid alanine ($NH_2CH_3CHCOOH$) adsorbed on metal surfaces can be regarded as a model system. Alanine on Cu(110) shows a rich phase diagram, including chiral and achiral organization of the molecules, which has triggered considerable interest in the atomic structure over the last decades [4–15]. However, despite the application of various surface science techniques such as low-energy electron diffraction (LEED), infrared reflection absorption spectroscopy (IRAS), x-ray photoelectron spectroscopy (XPS), photoelectron diffraction (PED), scanning-tunneling microscopy (STM), near-edge x-ray absorption fine structure (NEXAFS), and density functional theory (DFT), the detailed structure could not be cleared up. In this work, we have studied the atomic structure of phases with monolayer coverage and a (3×2) unit cell by means of grazing scattering of fast light atoms and molecules. For this system, we have demonstrated the application of the fast atom diffraction (FAD) method [16–18] to thin films of organic molecules recently [19]. In combination with triangulation techniques using fast atoms and LEED, the atomic structure of the topmost parts of the adsorbed molecules was investigated.

Alanine chemisorbs on the metal surface in its anionic form alaninate (NH_2CH_3CHCOO) by deprotonation of the carboxylic acid group. Depending on coverage, the bond to the substrate proceeds via the amino N atom and one or both of the O atoms of the carboxyl group as identified by IRAS measurements [4,5,7]. Long-range ordered phases are obtained after annealing of the saturated surface at temperatures above 360 K. Then, mainly a three-point binding configuration is present, where both oxygen atoms are bound to neighboring Cu atoms of a $[\bar{1}\,1\,0]$ row and the nitrogen atom to one substrate atom of the next close-packed row. Near-on-top positions were derived for all atoms from DFT calculations and PED studies [7,8,10], which makes two different orientations of the molecule possible, the so-called adsorption footprints.

For enantiopure alanine, i.e., pure enantiomers with single molecular handedness, a long-range order of adsorbates sets in for annealing temperatures above 430 K. For the phase III (in the notation of Ref. [7]), unit-cell vectors described by the matrix $(2,\bar{2};5,3)$ were identified on the basis of LEED data and alaninate molecules are arranged in chiral complexes consisting of six and eight molecules at the surface [5,7]. Annealing above 470 K leads to the achiral phase IV with (3×2) periodicity. For racemic alanine, i.e., an equal mixture of both enantiomers R- and S-alanine, the same unit cell is observed already for annealing at about 360 K. Striking features in LEED patterns for this phase are superstructure spots which are displaced in the $[\bar{1}\,1\,0]$ direction [11,12]. For racemic alanine the structure can be transferred into an undistorted "true" (3×2) phase IVb by dosing an additional amount of alanine. Annealing above 470 K results in the "distorted" phase IVa again. Desorption of the film is observed for temperatures above 520 K.

For all (3×2) phases the missing $(0\,m \pm 1/2)$ LEED spots are attributed to a glide-plane symmetry [7]. Since for enantiopure alanine the molecular chirality cannot be changed, only a "pseudo-glide-plane" symmetry can be present. Therefore it was assumed, in former studies, that two different adsorption footprints within a $p(3 \times 2)$ unit cell having this symmetry are the origin for the missing spots [7,8,10]. The footprints are illustrated by dashed triangles in one of the structural models from Ref. [14] shown in Fig. 1. In close analogy to the system $pg(3 \times 2)$glycine/Cu(110) [9,20], where a true glide-plane symmetry is possible, for each of the footprints two different structural modifications of the alaninate molecules were derived from DFT calculations [11,14]. The backbone of the molecule can be bent and the methyl group points outwards nearly perpendicular to the surface, or the molecular backbone is linear and the methyl group has a significant lateral

*Corresponding author: jan.seifert@physik.hu-berlin.de

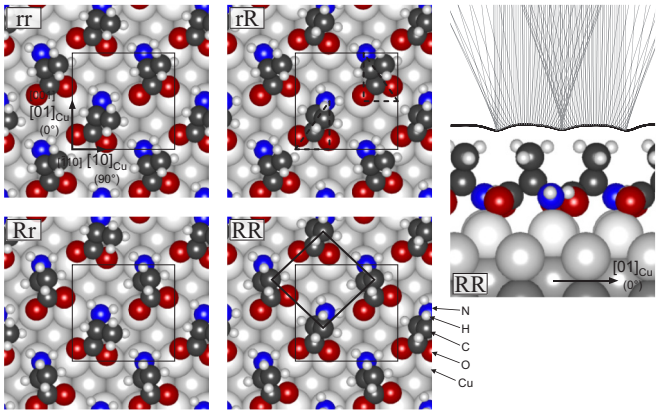

FIG. 1. (Color online) Left panels: Top view of structural models from Ref. [14] for enantiopure alaninate on Cu(110) with $p(3 \times 2)$ unit cells. In the panel of model rR the chiral adsorption footprints are indicated by triangles. They fulfill glide-plane symmetry observed with LEED, which cannot be given for two molecules of one enantiomer. Right panel: Side view of model RR, equipotential plane of averaged interaction potential with energy $E_\perp = 0.6$ eV and projected trajectories for scattering of He atoms with energy $E = 2$ keV and grazing incident angle $\Phi_{in} = 1^\circ$ in $[1\,0]_{Cu}$ direction. We use a superposition of atomic pair potentials; thus contour and trajectories are only estimates.

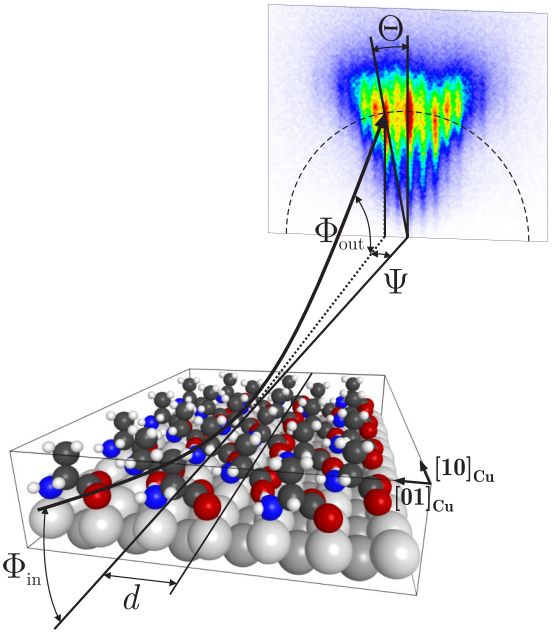

FIG. 3. (Color online) Sketch of scattering geometry.

displacement with respect to the rest of the molecule. The modifications were called "kinked" or "linear" in Ref. [11] and labeled with capital or small letters for each enantiomer in Ref. [14]. The structural models for enantiopure R-alanine and racemic alanine are shown in Figs. 1 and 2, respectively.

II. EXPERIMENTAL SETUP

In our experiments we have scattered H and He atoms as well as H_2 molecules with projectile energies $E =$ 0.2–2 keV from the adsorbate-covered surface under grazing angles of incidence Φ_{in} ranging from 0.2° to 1.8°, as sketched in Fig. 3. The projectile ions and molecules were produced in a Penning or electron cyclotron resonance (ECR) ion source and mass separated by means of an analyzing magnet.

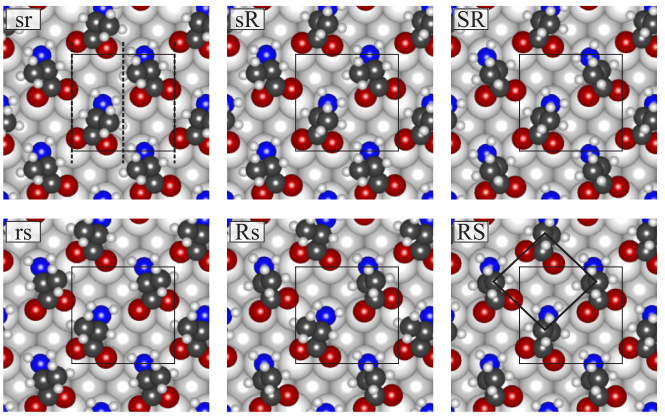

FIG. 2. (Color online) Structural models of racemic alaninate/Cu(110) from Ref. [14]. Glide-plane symmetry is given for models of left and right panels.

After neutralization in a gas target operated with helium for He projectiles or with krypton for H and H_2 projectiles and removal of residual ions using electric field plates, the beam was collimated by three sets of submillimeter slits to a divergence of about 0.01°. The slits served also as components of two differential pumping stages in order to maintain a pressure in the upper 10^{-11}-mbar domain in our UHV setup. The collimated beam is directed under grazing incidence onto the surface of the adsorbate-covered Cu(110) target mounted on a precision manipulator.

In front of the target a differentially pumped molecule evaporator is attached to the UHV chamber via a gate valve. Two resistively heated quartz glass containers—U shaped for evaporation from above—were filled with about 0.2 g of enantiopure S-alanine (99.5%) and R-alanine (99%) from Sigma-Aldrich [21]. The temperature of each evaporant is controlled by a thermocouple. Before evaporation, the alanine was outgassed up to 390 K for several hours. During sublimation the glass containers were held at about 400 K with a pressure of $p \approx 2 \times 10^{-6}$ mbar in the evaporator and $p \approx 2 \times 10^{-9}$ mbar in the UHV chamber.

The two-dimensional (2D) angular distributions of scattered projectiles were recorded by means of a position sensitive micro-channel-plate detector (MCP) [22] positioned 0.83 m behind the target. For light projectiles with an energy of 2 keV, the detection efficiency is about 50%, resulting from the geometrical open area of the channel plate [23]. Angular distributions and the resulting diffraction patterns can be recorded within a few minutes with a low flux of incident particles. Since the maximum counting rate of the complete detection system is limited to about 10^4 counts per second, the equivalent current of incident atoms is in the sub-fA regime and surface modifications caused by atom bombardment can be neglected here.

III. EXPERIMENTAL METHODS

For scattering along low-indexed axial channels formed by surface atoms, the effective projectile-surface interaction potential has axial symmetry with respect to individual strings of topmost surface atoms. This regime of "axial surface channeling" is characterized by a fast motion parallel to strings with energies $E_{\parallel} = E \times \cos^2 \Phi_{\text{in}}$ and a slow normal motion with energies $E_{\perp} = E \times \sin^2 \Phi_{\text{in}}$, where E is the total projectile energy. For grazing collisions ($\Phi_{\text{in}} \lesssim 2^\circ$) of kiloelectronvolt atoms or molecules, $E_{\perp}$ is in the subelectronvolt domain. The fast projectiles are steered by a large number of surface atoms, where the effective interaction potential results from an averaging along the axial surface channels [24,25]. The corrugation of the potential across the channels leads to an out-of-plane scattering denoted by the azimuthal angle Ψ in the surface plane or the deflection angle Θ in the detection plane (cf. Fig. 3). In the regime of classical scattering the intensity of scattered projectiles is enhanced at the maximum of angular deflection, the so-called collisional rainbow [26,27].

For sufficiently small angles of incidence and projectile energies, excitations of the solid are suppressed. Then quantum coherence is preserved and diffraction patterns can be observed (FAD) [16–18,28–42]. The azimuthal angle Ψ_n for diffraction spots of order n is related to the periodicity length $d_{[hk]}$ of the interaction potential normal to the axial channels formed by strings of surface atoms along the $[h\,k]$ direction and is given by the Bragg relation

$$d_{[hk]} \sin \Psi_n = n\lambda_{\text{dB}}, \tag{1}$$

with $\lambda_{\text{dB}} = h/Mv$ being the de Broglie wavelength associated with the center-of-gravity motion of a particle with mass M and velocity v, and h is Planck's constant. The de Broglie wavelength for 1 keV ^{4}He atoms is 0.0045 Å, almost 3 orders of magnitude smaller than the periodicity length d of the interaction potential. Therefore, the resulting splittings between Bragg peaks amount to typically 0.05° to 0.2° only. For quantum scattering the angular resolution in the experiment can be made so large that such small splittings can be resolved.

From the experimental angular splitting between adjacent diffraction spots $\Delta\Psi = \lambda_{\text{dB}}/d_{[hk]}$ one can obtain the periodicity interval $d_{[hk]}$ and from comparison with theoretical values for different surface directions the surface unit cell [36]. The averaging of the corrugation of the interaction potential along atomic strings [18] reduces the information on the surface symmetry to the direction $\boldsymbol{d}_{[h\,k]}$ perpendicular to the incident beam $\boldsymbol{r}_{[h\,k]} = h\boldsymbol{b_1} + k\boldsymbol{b_2}$, with h and k being indices of the supercell vectors $\boldsymbol{b_1}$ and $\boldsymbol{b_2}$. The lateral periodicity $d_{[h\,k]}$ is inversely proportional to the length of the reciprocal lattice vector of the supercell $\boldsymbol{g}_{[h\,k]} = h\boldsymbol{b}_1^* + k\boldsymbol{b}_2^*$ with reversed order of indices:

$$d_{[h\,k]_{(\boldsymbol{b_1},\boldsymbol{b_2})}} = \frac{|\boldsymbol{b_1} \times \boldsymbol{b_2}|}{|h\boldsymbol{b_1} + k\boldsymbol{b_2}|} = \frac{2\pi}{|\boldsymbol{g}_{[k\,\bar{h}]}|}. \tag{2}$$

The indices refer to the basis of the particular superstructure unit cell.

For triangulation measurements with fast atoms, 2D angular distributions were recorded during azimuthal rotation of the target in steps of 0.3°. After the measurement for individual azimuthal directions, the intensity in a small interval of angles close to the position of specular reflection $\Phi_{\text{out}} = \Phi_{\text{in}}$, $\Psi = 0^\circ$ is extracted and plotted as function of azimuthal angle for the rotation of the target. For scattering along axial channels of surface atoms, the projectiles are deflected from the direction of specular reflection which is dominant for random azimuthal orientation of the target. This results in dips in the intensity of specularly scattered particles whenever the atom beam is scattered along axial channels in the surface plane. Details on this variant of triangulation method will be given elsewhere [43].

Scattering of H atoms with energies of some 10 keV results in a considerable emission of electrons. The number of electrons changes upon azimuthal rotation of the target, which was used as an alternative detection for the triangulation method (ion-beam triangulation, IBT) [42,44–46]. The number of target electrons emitted per scattering event was detected by means of a surface barrier detector [47,48] biased to high voltage of about 20 kV. By selecting fractions of low electron numbers, electrons emitted by projectiles scattered in front of the surface are recorded. Also for this method of detection, axial channels are identified by dips of the signal during azimuthal rotation of the target.

IV. SURFACE PREPARATION

The copper substrate was prepared by cycles of grazing sputtering with 25 keV Ar^+ ions and subsequent annealing at about 790 K for 20 min. In the final state of preparation no impurity atoms could be detected via Auger electron spectroscopy (AES) and the LEED pattern showed a well-defined (1×1) structure [Fig. 4(a)]. As demonstrated for Ag and Ni surfaces, quantum scattering at clean metal surfaces are in general limited to low energies and small incidence angles, because interactions of projectiles with the electron gas lead to electronic excitations and, thus, to loss of coherence [28,31,39]. As shown in the 2D intensity distributions in Figs. 4(b) and 4(c) for scattering of 1 keV He atoms in $[1\,0]_{\text{Cu}}$ direction [49], diffraction phenomena can be observed for the clean Cu(110) surface. The lateral periodicity length $d_{[1\,0]_{\text{Cu}}} = (3.59 \pm 0.06)$ Å derived from the azimuthal peak splitting at various projectile energies and incidence angles is in line with the expected value of the lattice constant $a_{\text{Cu}} = 3.615$ Å [50].

Alaninate overlayers were prepared by exposing the clean Cu(110) surface to one of the enantiomers or to the racemat by coevaporation of R- and S-alanine. In order to study the growth process and to adjust the adsorption rates, we recorded the specular intensity of 2 keV He atoms grazingly scattered from the surface during deposition of alanine [38,51,52]. The intensity curves shown in Fig. 5 exhibit a pronounced drop close to zero, after the shutter to the main chamber is opened, indicating disorder at the surface. Then the intensity increased again and reached a maximum after about 10 min of exposure, which can be assigned to a completed monolayer. Afterwards the specular intensity decreased continuously for adsorption at room temperature and levels off at higher target temperatures, where pileup of molecules is suppressed and adsorbates are better ordered. This growth behavior was the same for both enantiomers and the racemat. For coevaporation of R- and

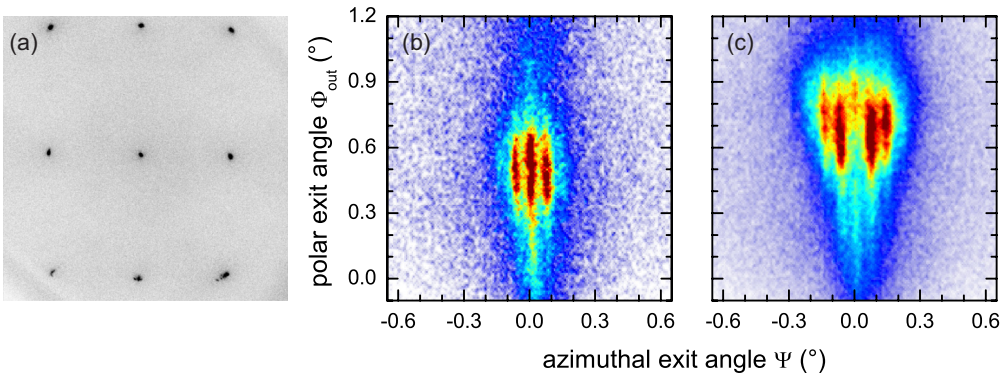

FIG. 4. (Color online) LEED image ($E_e = 120$ eV) (a) and intensity distributions of 1 keV He atoms scattered in $[1\,0]_{Cu}$ direction from clean Cu(110) surface for incident angle of $\Phi_{in} = 0.5°$ (b) and 0.7° (c).

S-alanine with individually calibrated evaporators, the growth rate was approximately doubled (green curve in Fig. 5). From the variation of time for the maximum of specular intensity, a mixing ratio of $(50 \pm 5)\%$ is estimated.

For the preparation of ordered phases of alaninate, the saturated surface was annealed in UHV at temperatures between $T_a = 370$–460 K for 7 min. Figure 6 shows the LEED patterns of the chiral phase III and the achiral phase IV of both enantiomers, and the phases IVa and IVb of the racemat as observed in previous studies. For a temperature of $T_a \approx 430$ K a transition from phase III to IV takes place. Desorption starts at about 460 K. These temperatures agree with the values in Refs. [11,13], but are about 40 K too low compared to Refs. [7,12].

V. STRUCTURE DETERMINATION

A. Surface unit cell

In Fig. 7 we show 2D angular distributions for the intensities of scattered projectiles obtained for 0.6 keV H atoms and 0.3 keV H_2 molecules after interaction with enantiopure S and racemic alaninate on Cu(110) phase IVb for three different azimuthal orientations of the target. The de Broglie wavelength for all projectiles amounts to $\lambda_{dB} = 0.012$ Å so that the splittings of diffraction spots are the same for H_2 and H. The polar incidence angle is $\Phi_{in} = 0.6°$. In the left and right panels the projectile beam was aligned parallel to the low-indexed substrate directions $[1\ 0]_{Cu}$ and $[0\ 1]_{Cu}$, respectively. The diffraction patterns in the middle panels of Fig. 7 were recorded for an azimuthal rotation of the target by $\Gamma = 46.5°$ from $[0\ 1]_{Cu}$. This corresponds to $[3\ 2]_{Cu}$, the diagonal of the $p(3 \times 2)$ unit cell and, when considering a $c(3 \times 2)$ unit cell of the adsorbate, to $[1\ 0]_{ala}$ (see Fig. 8). The diffraction patterns for the $[0\ 1]_{ala}$ direction (not shown) are almost identical to those for $[1\,0]_{ala}$. The intensity distributions for the enantiopure phase IV (lower panels), for the racemic phase IVb (middle panels), and the racemic phase IVa (not shown) are very similar for the same projectiles. Due to the axial symmetry of the scattering potential along atomic chains at the surface, the diffraction patterns are positioned on an annulus. Compared to FAD studies on near-perfect surfaces, the reflexes are elongated in polar direction for the alaninate-covered surface. This points to contributions of disorder at the surface, as also observed via STM [12], resulting in a closer approach of

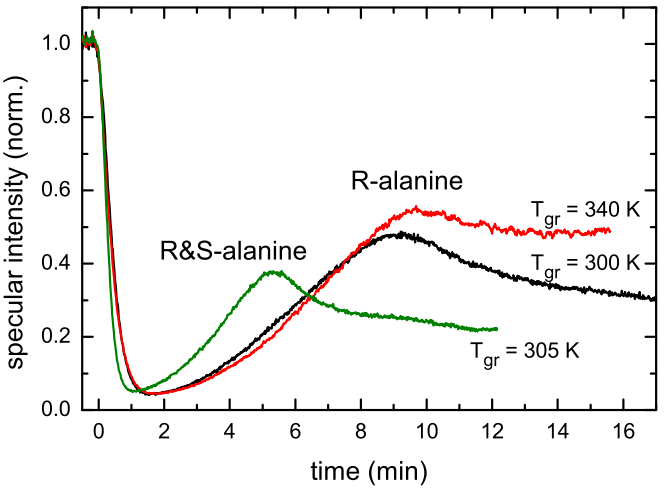

FIG. 5. (Color online) Specular intensity of 2 keV He atoms grazingly scattered from the Cu(110) surface during deposition of enantiopure R- and racemic R&S-alanine at target temperatures as indicated.

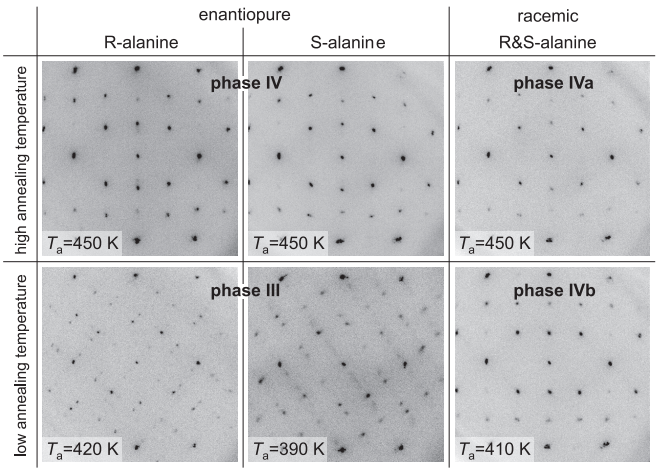

FIG. 6. LEED images ($E_e = 120$ eV) of enantiopure R- and S-alanine as well as racemic alanine after annealing the saturated surface for 7 min at temperatures as indicated.

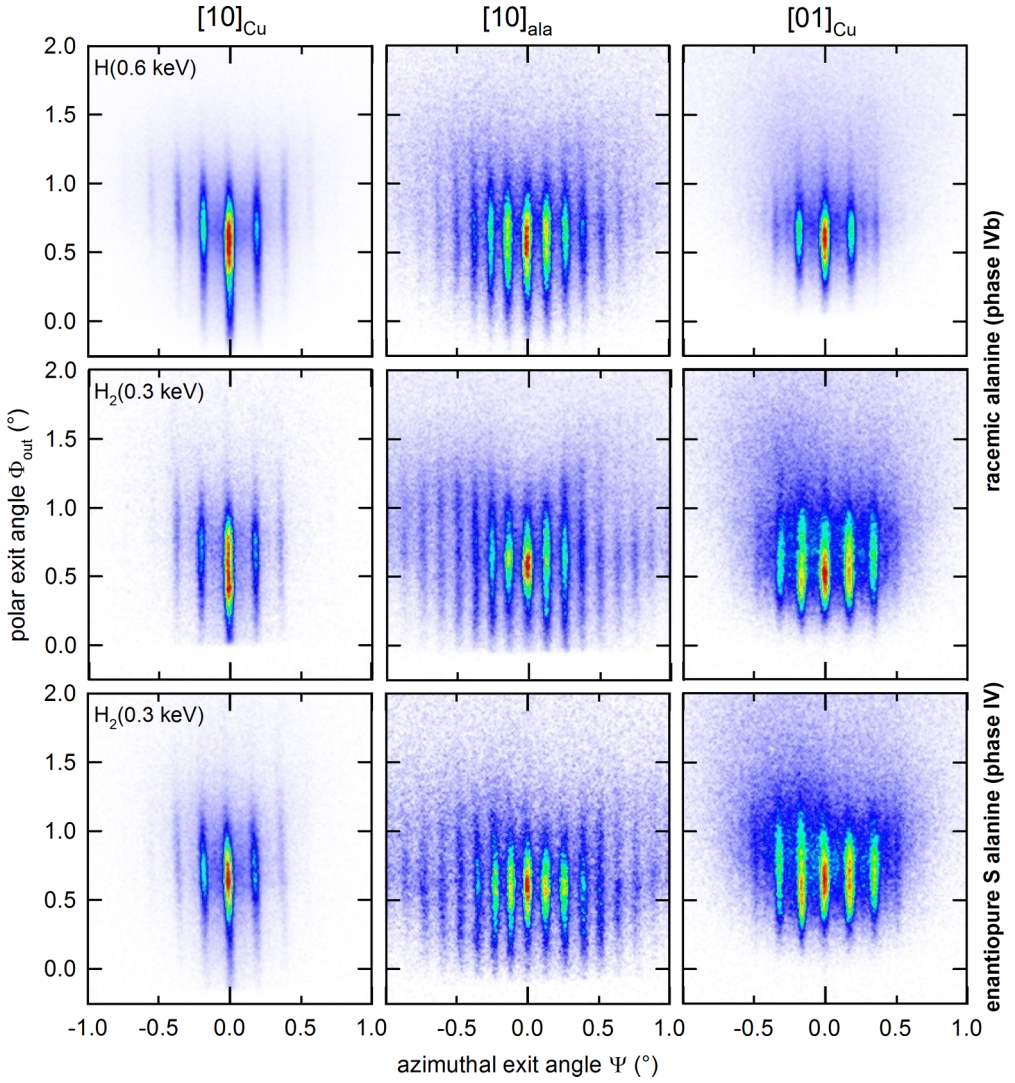

FIG. 7. (Color online) Angular distributions of scattered H atoms (projectile energy $E = 0.6$ keV, upper panels) and H_2 molecules ($E = 0.3$ keV, middle and lower panels) with de Broglie wavelength $\lambda_{dB} = 0.012$ Å and incident angle $\Phi_{in} = 0.6^\circ$ from racemic alaninate phase IVb (upper and middle panels) and enantiopure S-alaninate phase IV (lower panels) on Cu(110) for the azimuthal directions $[1\,0]_{Cu}$, $[1\,0]_{ala}$, and $[0\,1]_{Cu}$ (from left to right).

projectiles to thermally displaced surface atoms and enhanced angular scattering. In the azimuthal direction, defined Bragg reflexes are observed, which allows one to determine symmetry widths of the surface unit cell. Aside from a gradual reduction

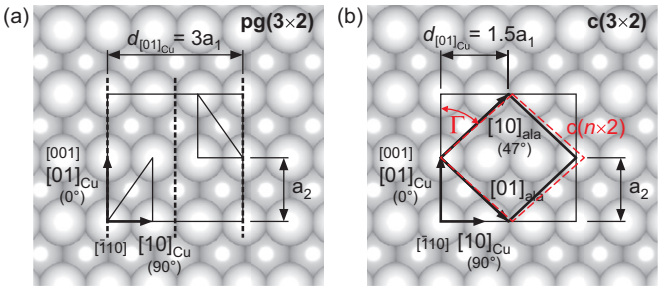

FIG. 8. (Color online) Sketch of channel widths for scattering in $[1\,0]_{Cu}$ and $[0\,1]_{Cu}$ surface direction for an (a) $pg(3 \times 2)$ and (b) $c(3 \times 2)$ unit cell on a Cu(110) surface.

of diffraction intensities with the azimuthal scattering angle Ψ, we found no intensity modulation of neighboring diffraction spots. Therefore information on atomic positions within the unit cell cannot be derived from the data. This holds also for a variation of the projectile energy, as apparent from the diffraction charts [18] shown in Figs. 9(a) and 9(c) for scattering from racemic alaninate/Cu(110) phase IVb along $[0\,1]_{Cu}$ and $[1\,0]_{ala}$, respectively. The intensities of the angular distributions close to the annulus for elastic scattering, as illustrated in Fig. 3 for various energies and resulting de Broglie wavelengths, are plotted color-coded as a function of λ_{dB} and deflection angle Θ. The intensities of individual Bragg peaks are determined by interference within a unit cell and depend on the de Broglie wavelength of the normal motion $\lambda_{dB\perp}$. Here the polar angular spread of scattered particles is so large that the different intensities are washed out, or the coherence of trajectories within one unit cell is suppressed due to the mentioned degree of disorder at the surface. An analysis of peak intensities in terms of the

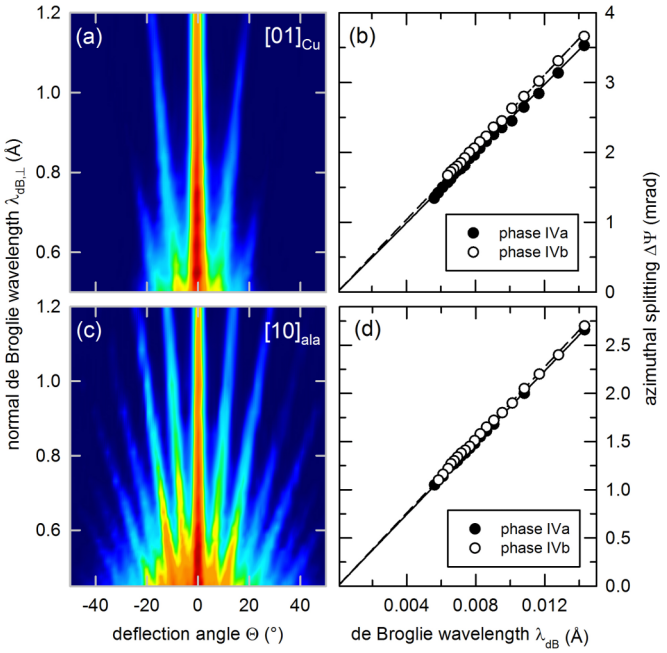

FIG. 9. (Color online) Diffraction charts (left panels) derived from azimuthal intensity distributions for various measurements with different projectile energy and de Broglie wavelength for scattering of H_2 molecules in $[0\,1]_{Cu}$ (upper panels) and $[1\,0]_{ala}$ (lower panels) direction from racemic phase IVb as well as azimuthal peak splitting as a function of de Broglie wavelength (right panels).

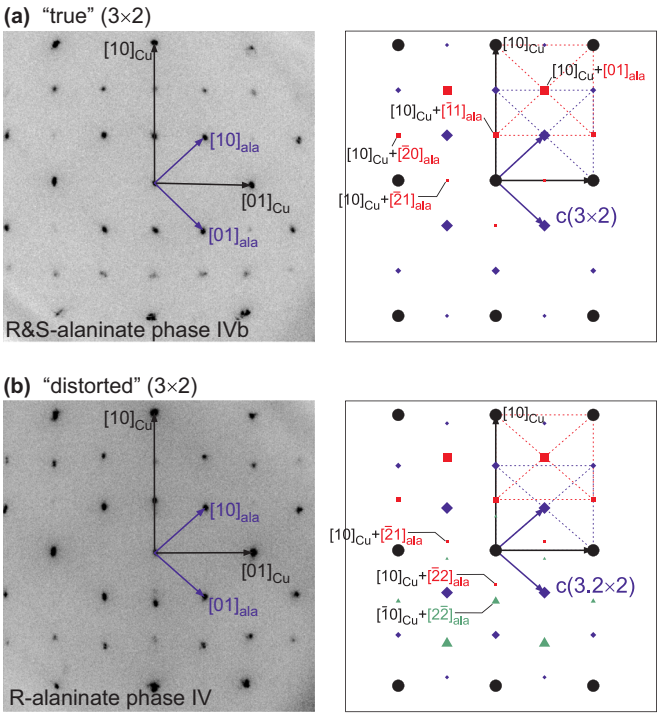

FIG. 10. (Color online) LEED patterns and schematic representations of diffraction spots using a center symmetric unit cell for an (a) "true" (3 × 2) unit cell of racemic phase IVb and (b) "distorted" (3 × 2) unit cell of enantiopure phase IV of alaninate/Cu(110). The second case holds also for the racemic phase IVa (not shown here, cf. Ref. [19]).

corrugation of the interaction potentials across axial channels was not possible here. However, slightly different intensities of adjacent diffraction orders were observed for 1 keV H_2 molecules, as shown in Fig. 3, so that in principle such analysis might be feasible also for films of organic molecules.

From best fits with Lorentzian line shape to individual diffraction spots for scattered H and He atoms as well as H_2 molecules at various projectile energies, we derived the azimuthal splitting $\Delta\Psi$ and via the Bragg relation [Eq. (1)] the lateral periodicity length of the surface d. For scattering along the $[1\ 0]_{Cu}$ direction we obtained $d_{[1\,0]_{Cu}} = (3.64 \pm 0.07)$ Å. A $p(3 \times 2)$ unit cell would result in a doubled value $2a_2 = 7.22$ Å. This discrepancy can be attributed to the presence of glide-plane symmetry $pg(3 \times 2)$, as discussed in literature (cf. Fig. 8). According to Eq. (2), halving of d leads to a doubling of the interval between diffraction spots, as observed in the LEED pattern (Fig. 6) in $[0\,1]_{Cu}$ reciprocal lattice direction and missing $(0\ m+1/2)$ spots. However, for scattering in $[0\,1]_{Cu}$ direction, $d_{[0\,1]_{Cu}} = (3.86 \pm 0.07)$ Å is obtained, which is half of the expected $3a_1 = 7.67$ Å. The deviation of the symmetry width from a $p(3 \times 2)$ unit cell for both surface directions can be explained by a $c(3 \times 2)$ unit cell, only (cf. Fig. 8). The resulting $d_{[1\,0]_{ala}} = (5.30 \pm 0.05)$ Å for the diagonal direction along $[1\ 0]_{ala}$ is in line with all (3×2) unit cells.

Also the LEED patterns can be interpreted with a $c(3 \times 2)$ symmetry, if multiple scattering is taken into account. Electrons scattered from the substrate are scattered a second time by the adsorbate. Diffraction from the substrate in any $[k\,l]_{Cu}$ direction results in shifted diffraction patterns of the adsorbate [here $c(3 \times 2)$] with its origin at the substrate reciprocal lattice points $[k\,l]_{Cu}$ [53]. In Fig. 10(a) the LEED pattern for racemic alaninate phase IVb is compared to a schematic representation of the diffraction spots. The basis vectors of the adsorbate are plotted in blue color and the corresponding reciprocal lattice points by blue diamond symbols. The red squares illustrate diffraction spots originating from double scattering from the substrate in $[1\ 0]_{Cu}$ direction and from the adsorbate. In this way the positions of all diffraction spots can be reproduced by a $c(3 \times 2)$ unit cell. With increasing length of the reciprocal lattice vector the diffraction intensity is reduced. This explains at least qualitatively the reduced intensity of some LEED spots as $(1\,0)_{Cu} + (\bar{2}\,0)_{ala}$. It holds also for the $(1\,0)_{Cu} + (\bar{2}\,1)_{ala}$, which corresponds to the missing spot $[0\,m+1/2]_{Cu}$ attributed to a glide-plane symmetry so far [7]. However, in Refs. [12,13] a faint spot at this position can be identified which supports a $c(3 \times 2)$ symmetry.

The origin of the displacements of LEED spots for the alaninate phases IV (enantiopure) and IVa (racemic) has not been understood so far. Possible explanations were based on the reconstruction of the substrate [7] or a large long-range periodicity, where a local $p(3 \times 2)$ arrangement enhances the intensity of spots in the vicinity of $p(3 \times 2)$ lattice points [11,14]. On the basis of a unit cell with centered symmetry, the "distorted" LEED patterns can be explained in a straightforward manner. If the unit cell is expanded in $[1\,0]_{Cu}$ direction by about 6%, the LEED spots originating solely from the adsorbate layer [blue diamonds in Fig. 10(b)] are closer to the [0 0] spot and the LEED spots stemming from

TABLE I. Parameter n of the unit-cell size $c(n \times 2)$ for different alaninate phases on Cu(110). The values for the FAD measurements were derived from the periodicity interval d for scattering in $[0\,1]_{Cu}$ direction. The values for the triangulation method are derived from the azimuthal angle Γ of the $[1\,0]_{ala}$ axial channel with respect to $[0\,1]_{Cu}$.

Alaninate phase	LEED	FAD		Triangulation	
R-alaninate IV	$n = 3.15 \pm 0.04$			$\Gamma = (48.3 \pm 0.4)^\circ$	$n = 3.17 \pm 0.04$
S-alaninate IV	$n = 3.18 \pm 0.02$	$d_{[01]_{Cu}} = (4.00 \pm 0.08)$ Å	$n = 3.13 \pm 0.06$	$\Gamma = (48.2 \pm 0.4)^\circ$	$n = 3.16 \pm 0.04$
R&S-alaninate IVa	$n = 3.15 \pm 0.06$	$d_{[01]_{Cu}} = (4.04 \pm 0.09)$ Å	$n = 3.16 \pm 0.07$	$\Gamma = (47.8 \pm 0.4)^\circ$	$n = 3.12 \pm 0.04$
R&S-alaninate IVb	$n = 2.99 \pm 0.03$	$d_{[01]_{Cu}} = (3.86 \pm 0.07)$ Å	$n = 3.02 \pm 0.05$	$\Gamma = (46.3 \pm 0.4)^\circ$	$n = 2.96 \pm 0.04$

double scattering from the substrate (for example, in $[1\,0]_{Cu}$ direction) and adsorbate (red squares) are shifted away from the [0 0] spot. This leads to the observed zig-zag distortion. From the spot positions for various LEED patterns we derive a unit-cell size of $c[(3.18 \pm 0.02) \times 2]$ for S-alaninate and $c[(3.15 \pm 0.04) \times 2]$ for R-alaninate. For the undistorted racemic alaninate phase IVb a value of $c[(2.99 \pm 0.03) \times 2]$ is obtained. This latter phase can be gradually transferred into the distorted phase IVa by stepwise annealing. After a maximum annealing temperature of $T = 450$ K, a $c[(3.15 \pm 0.06) \times 2]$ unit-cell size follows from the LEED analysis. A systematic enlargement of the unit cell in $[1\,0]_{Cu} = [\bar{1}\,1\,0]$ direction is present also in STM studies by Haq *et al.* for the racemic phase IVa [Fig. 8(b) in Ref. [12]].

In the LEED pattern in Fig. 10(b), faint $(1\,0)_{Cu} + (\bar{2}\,2)_{ala}$ reflexes can be identified which are present also in patterns reported in Refs. [7,12] as well as the $(1\,0)_{Cu} + (\bar{2}\,1)_{ala}$ reflexes. This gives evidence for the interpretation of the distortions in the LEED patterns via a $c(3.16 \times 2)$ unit cell and multiple scattering. The enlargement of the unit cell follows also from the FAD measurements. The splitting of the diffraction spots decreases for scattering in $[0\,1]_{Cu}$ direction when the racemic phase IVb without distortions [full circles in Fig. 9(b)] is annealed at temperatures above 430 K, resulting in the phase IVa with distortions (open circles). From the slope of the splitting $\Delta\Psi$ as a function of λ_{dB}, a lateral periodicity of $d_{[0\,1]_{Cu}} = (4.04 \pm 0.09)$ Å is derived, which corresponds to a $c[(3.16 \pm 0.07) \times 2]$ unit cell, while $d_{[1\,0]_{Cu}}$ remains unchanged (see Ref. [19]). For scattering along the (diagonal) direction $[1\,0]_{ala}$ one is less sensitive to an expansion in $[1\,0]_{Cu}$ direction and the change of splittings can hardly be resolved [Fig. 9(d)]. However, the parameter $n = 3.14 \pm 0.09$ of the $c(n \times 2)$ unit cell is consistent with the result for $[0\,1]_{Cu}$ scattering direction. The values of all phases are listed in Table I and agree well with the values obtained from LEED.

The enhanced length of the unit cell in one direction also leads to a slight azimuthal rotation of the diagonal of a $p(3 \times 2)$ unit cell which is the direction of the basis vector of a $c(3 \times 2)$ adsorbate unit cell $[1\,0]_{ala}$. The angle Γ for this direction with respect to $[0\,1]_{Cu}$ is given by $\tan\Gamma = n/2\sqrt{2}$ for a $c(n \times 2)$ unit cell (cf. Fig. 8). For the undistorted phase this amounts to $\Gamma = 46.7^\circ$, and for the phase with a $c(3.16 \times 2)$ unit cell to $\Gamma = 48.2^\circ$. The resulting shift of the azimuthal angle $\Delta\Gamma = 1.5^\circ$ considerably changes the scattering geometry for fast atom diffraction. In Ref. [34] we have demonstrated the effect of an azimuthal misalignment of the atomic beam with respect to a low-indexed crystal direction on the diffraction pattern, which was studied theoretically and confirmed experimentally [37,40,41]. The same effect is observed when the direction of the atomic chains at the surface is changed due to a temperature-induced expansion of the unit cell from $c(3 \times 2)$ to $c(3.16 \times 2)$, i.e., the transition from phase IVb to phase IVa [Figs. 11(a) and 11(b)]. After the target is rotated by 1.6°, the atomic beam is parallel again to the shifted axial channel and a similar diffraction pattern can be observed for both phases [Fig. 11(c)].

Similar results were also observed for classical scattering with 2 keV He atoms. In Fig. 12 we show angular distributions for scattering along three main azimuthal directions from the alaninate-covered surface (upper panels) and the clean Cu(110) surface (lower panels). For scattering along $[1\,0]_{ala}$

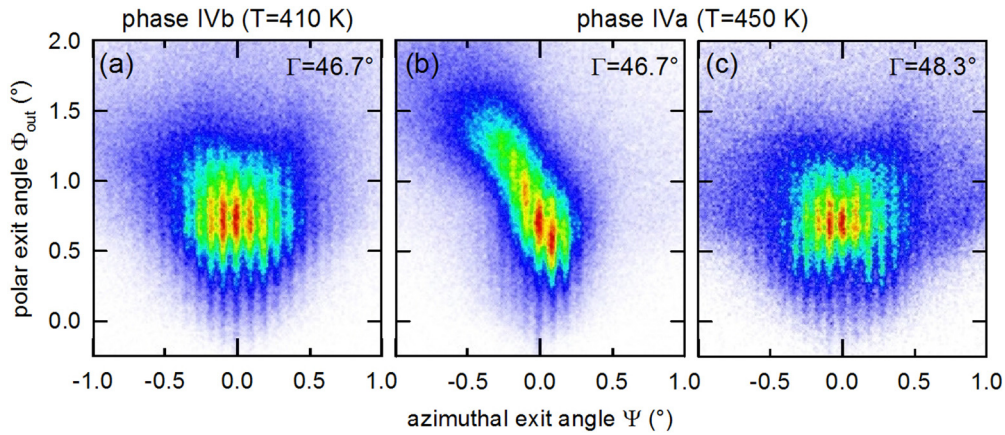

FIG. 11. (Color online) Intensity distributions for scattering of 0.7 keV H_2 molecules from the surface of racemic alaninate phase IVb (a) and IVa (b) and (c) for azimuth angles Γ with respect to $[0\,1]_{Cu}$ as indicated.

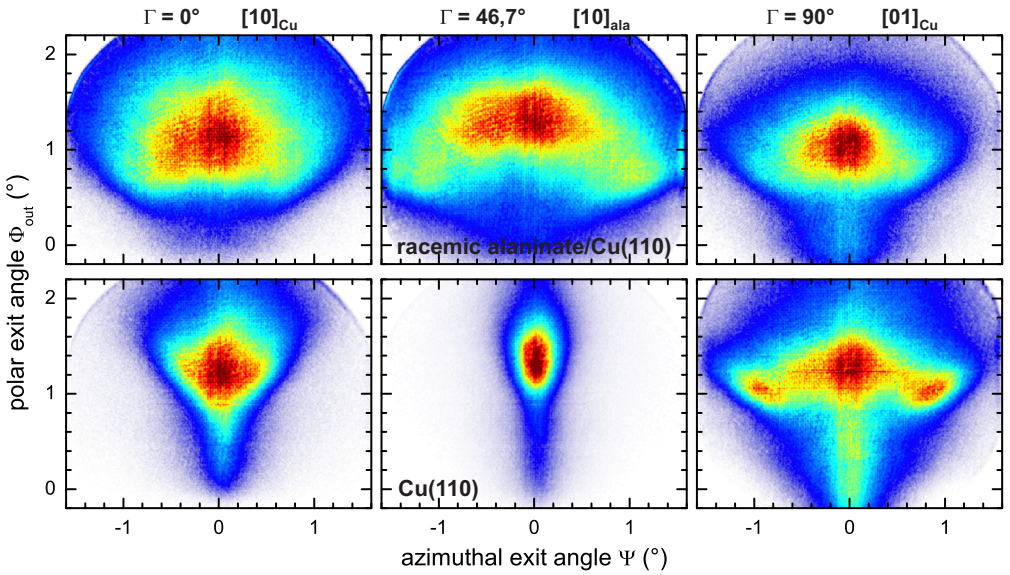

FIG. 12. (Color online) Angular distributions of scattered 2 keV He atoms ($\Phi_{in} = 1.2°$) from racemic alaninate/Cu(110) phase IVb (upper panels) and from clean substrate (lower panels) along three azimuthal directions.

($\Gamma = 46.7°$), a large rainbow angle corresponding to a wide axial surface channel can be observed for the adsorbate, while for the substrate nearly specular reflection corresponding to planar surface channeling for the relatively high-indexed surface direction $[3\,2]_{Cu}$ is present. Despite that angular distributions for the adsorbate are not as well defined as for the substrate, for some directions axial channels can be identified. When the intensity in the vicinity of specular reflection is extracted from the 2D distributions recorded during azimuthal rotation of the target, triangulation curves can be generated. In Fig. 13 the specular intensity for scattering from the substrate and different phases IV are plotted as a function of the azimuthal angle Γ with respect to the $[0\,1]_{Cu}$ surface channel. For the clean copper surface the low-indexed directions of a fcc(110) surface can be identified. For alaninate/Cu(110) phase IV, the axial channel along $[1\,1]_{Cu}$ has fully disappeared, which demonstrates the surface sensitivity of this technique. Instead, the largest decrease of the specular intensity is present for the $[1\,0]_{ala}$ axial channel. Since the widest axial channel is usually observed for scattering along the basis vector of the surface unit cell, this is a further hint for an arrangement of topmost atoms in a $c(3 \times 2)$ unit cell. The curves for enantiopure R- and S-alaninate are almost identical, which confirms the achiral assembly of molecules for this phase. Also, the curves for racemic alaninate are similar, but for the phase IVb with undistorted LEED pattern a shift of the $[1\,0]_{ala}$ axial channel compared to the distorted phases by about $\Delta\Gamma = 1.5°$ is evident. From the azimuthal angle Γ of this axial channel one can derive the values n of the $c(n \times 2)$ unit cell for all phases which are summarized in Table I. The analysis confirms the results from LEED and FAD.

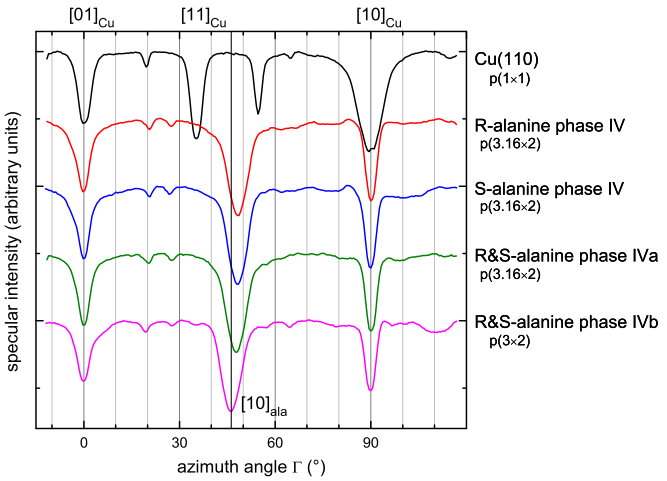

FIG. 13. (Color online) Triangulation curves for alaninate adsorbates and clean substrate derived from specular intensity of angular distributions as shown in Fig. 12 (2 keV He atoms, $\Phi_{in} = 1.2°$) as a function of azimuthal orientation of the target.

The results from LEED, FAD, and triangulation imply a center symmetrical unit cell, enlarged in one direction for phases IV and IVa. However, a full center symmetry of the substrate and the adsorbate is not possible, since for the racemat both types of alanine have to be present, but one unit cell contains only one molecule. For neighboring $c(n \times 2)$ unit cells, the registry to the substrate changes by $n/2 \approx 1.5$–1.6 lattice spacings in $[1\,0]_{Cu}$ direction, i.e., from atop to bridge adsorption sites. Therefore, center symmetry can be attributed only to parts of the surface as a possible glide-plane symmetry to the enantiomer (see, e.g., Ref. [7]).

B. Atomic structure

For a detailed analysis of the triangulation curves, we performed trajectory computer simulations based on classical mechanics and analyzed the fractions of specularly reflected projectiles as a function of the azimuthal rotation of the target surface. In Fig. 14 the resulting triangulation curves for the

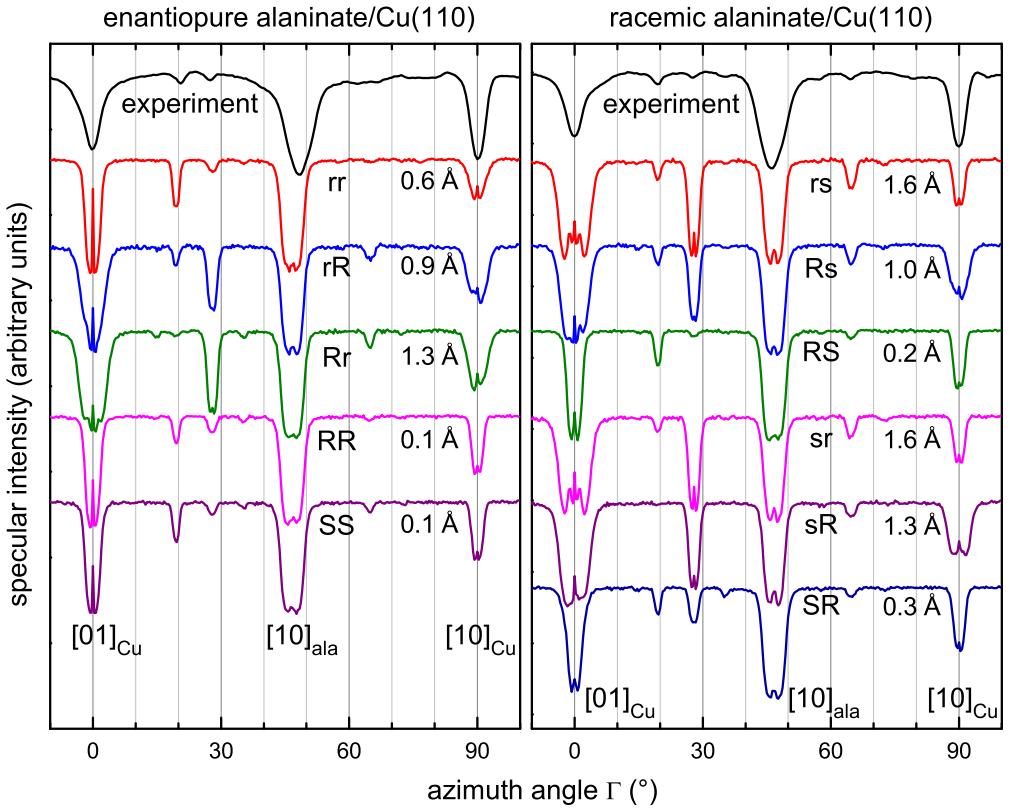

FIG. 14. (Color online) Experimental and simulated triangulation curves for enantiopure and racemic alaninate/Cu(110) for the models of Ref. [14] shown in Figs. 1 and 2. The deviations of the position of methyl groups from a centered unit cell are indicated (for details see text).

structural models from Ref. [14] shown in Figs. 1 and 2 are compared with the experiment. The principal directions are reproduced by all models, but for enantiopure alanine the $[1\,0]_{ala}$ direction of the simulations is not shifted to a higher angle Γ as for the experiment, since all models assume a $p(3 \times 2)$ unit cell. However, an expanded unit cell affects only the peak positions and not their intensities, and the corresponding directions of simulation and experiment can be compared directly. The relevant features are the surface channels for $\Gamma = 20^\circ$ and 29°. The models rR, Rr, rs, Rs, sr, and sR can be excluded, since a large reduction of the specular intensity is not observed in the experiment for $\Gamma = 29^\circ$. Since we used only simple interatomic potentials [54] and assumptions on thermal displacements of atoms, we cannot differentiate between the remaining models rr and RR for the enantiomere and RS and SR for the racemat. A coexistence of these arrangements is also possible from the results of grazing atom scattering.

The low energy of the motion normal to the surface of $E_\perp = 0.6$ eV ensures scattering of the helium atoms in front of the adsorbed molecules (see Fig. 1). Then projectile trajectories are determined by atoms of the methyl groups. In Fig. 14, we specify for the individual structural models the distance of the position of one methyl group of the $p(3 \times 2)$ unit cell to the position of the second methyl group shifted by the basis vector of the centered unit cell. It becomes apparent that the agreement between experiment and simulation is determined by the deviation of methyl group positions from a center symmetrical $c(3 \times 2)$ unit cell. The lowest value and good agreement of triangulation curves is found for the model RR for which a centered unit cell is drawn in Fig. 1. This holds for model RS for racemic alanine.

For projectile energies less than a few kiloelectronvolts, the information on atomic positions is limited to the atoms of the topmost 1 Å, i.e., the methyl group. One cannot distinguish between different adsorption sites. In DFT and photoelectron diffraction studies, roughly on-top positions of oxygen and nitrogen or at least binding to only one copper atom were concluded [7,8,10]. In literature only a $p(3 \times 2)$ unit cell with one or two molecules and no incommensurate fitting of superstructure and substrate was tested. In DFT studies from Blanco-Rey and Jones [14], it was shown that also for a reduced coverage of $\Theta = 3/10$, on-top positions are energetically favored. Therefore a uniformly spaced arrangement of molecules with distance $n\,a_1$ in $[1\,0]_{Cu}$ direction for a $c(n \times 2)$ unit cell including bridge sites seems to be unlikely. To maintain the preferred adsorption sites also for a $c(3.16 \times 2)$ arrangement of the methyl groups, drastic reconstruction of the substrate or a modification of the alaninate molecule is necessary. The first case can be discarded from the results of triangulation measurements, where the electron emission induced by fast hydrogen atoms is recorded (ion-beam triangulation). In Fig. 15, we show the results for the substrate and the adsorbate-covered surface with the "distorted" phase IV of R-alaninate. The data represents the fraction of events with only a low number of emitted electrons ($\lesssim$5) per scattered 25 keV H atom. Aside from an overall reduced intensity of the signals for the adsorbate,

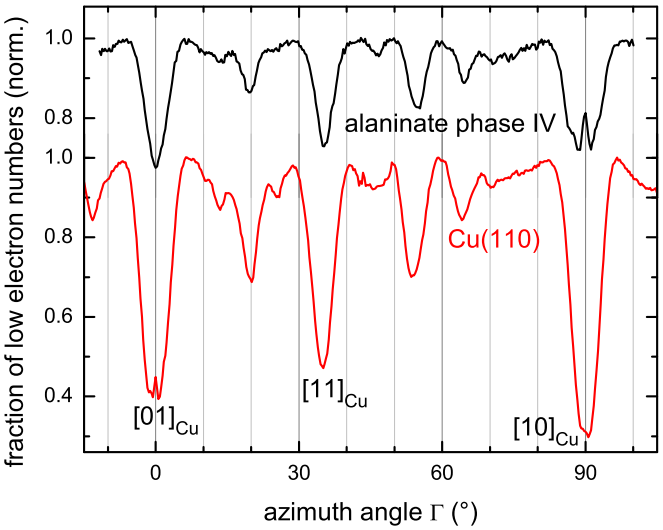

FIG. 15. (Color online) Triangulation curves derived from events with low numbers of emitted electrons for scattering of 25 keV hydrogen atoms from R-alaninate (phase IV) covered and clean Cu(110) surface.

both curves are very similar and exhibit dip positions and heights for a simple unreconstructed fcc(110) surface. The fast projectiles seem to be only weakly affected by the adsorbate atoms or do not contribute to the electron emission for an azimuthal rotation of the target. The information from this type of triangulation is limited to the topmost copper atoms, which cannot be significantly displaced laterally, especially not with a continuously increased spacing of 3.16/3 unit cells in $[1\,0]_{\mathrm{Cu}} = [\bar{1}\,1\,0]$ direction. This would result in a shift of the azimuthal direction of the $[1\,1]_{\mathrm{Cu}}$ channel from $\Gamma = 35.3^{\circ}$ to 36.7° which is not observed in the experiment.

A $c(3.16 \times 2)$ arrangement of the methyl groups and the preferred on-top adsorption sites are possible for small deformations of the alaninate molecules. From DFT calculations [11,14], two different modifications for each enantiomer were derived, where the methyl groups have significant lateral displacements with respect to the rest of the molecule (see Figs. 1 and 2). With two adsorption footprints, four modifications of each enantiomer are possible. The position of the methyl group varies in $[1\,0]_{\mathrm{Cu}}$ direction by about 2.5 Å with respect to the adsorption site of the molecule. Due to an alternating molecular footprint and modification an arrangement of molecules with adsorption on the preferred on-top sites with local $p(3 \times 2)$ symmetry and at the same time a spacing of the protruding methyl groups of ≈3.16 substrate unit cells [resulting in the observed $c(3.16 \times 2)$ symmetry] is possible. For the racemat the methyl group positions can vary also due to the sequence of the two enantiomers. In the DFT calculations [11,14], similar adsorption energies were derived for all combinations of molecular modifications within a $p(3 \times 2)$ unit cell. It was concluded that intermolecular interactions prevail over footprint and enantiomeric effects on the surface stress, which is compressive in $[1\,0]_{\mathrm{Cu}} = [\bar{1}\,1\,0]$ direction and thus favors a reduced coverage. However, the applied functionals do not account for dispersion, i.e., van der Waals interactions [14]. We cannot estimate the strength of interaction between adjacent methyl groups, but it seems to be the driving force for their equidistant spacing, which is systematically increased for phases IV and IVa, and consequently for the different molecular modifications. The influence of methyl groups on the assembly of molecules is assumed to be a key factor also for alanine on further Cu surfaces [15] and may be important for other adsorbate systems such as acetate/Cu(110) [55]. We note that disregarding the preferred on-top adsorption sites described in literature, a continuous spacing of the whole molecule by 3.16 unit cells in the $[1\,0]_{\mathrm{Cu}}$ direction is also possible on the basis of our measurements.

In Fig. 16, we show a simplified structural model for enantiopure R-alaninate on Cu(110). The different configurations of adsorbate molecules in the DFT-optimized models from Ref. [14] are rearranged in a way that the adsorption sites remain unchanged but the methyl groups occupy nearly the corners of a $c(3.2 \times 2)$ lattice. This results in a reduced coverage of $\Theta = 1/3.2$, a change of the chiral footprint sequence after five alaninate molecules as indicated by triangles, and a large effective unit cell $c(16 \times 2)$. With this procedure, also incommensurate $c(3.16 \times 2)$ unit cells can be produced and thus also the continuous transition from a $c(3 \times 2)$ (phase IVb) to a $c(3.16 \times 2)$ unit cell (phase IVa) observed for increasing annealing temperatures for racemic alaninate can be explained. A larger unit cell with local $p(3 \times 2)$ adsorption geometry is also the basis for the model RrR studied in Ref. [14] and for an explanation of distortions in the LEED images [11,14].

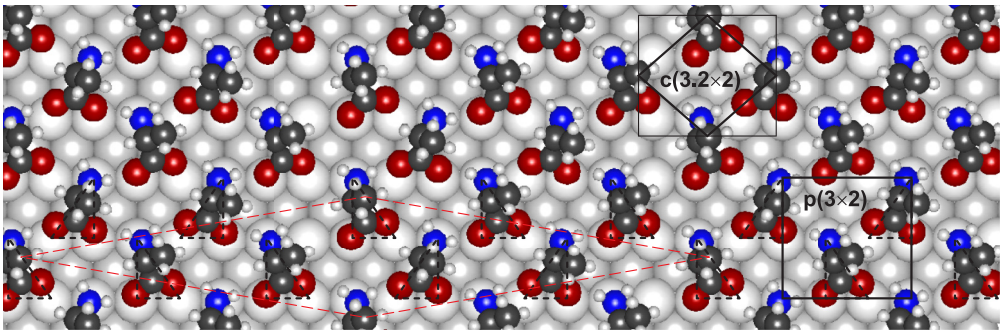

FIG. 16. (Color online) Structural model of enantiopure R-alaninate in "distorted" phase IV with reduced coverage and change of sequence of chiral footprints. Molecules are bound to the substrate locally in a $p(3 \times 2)$ unit cell, but the methyl groups are arranged in an elongated $c(3.2 \times 2)$ unit cell.

Compared to grazing atom scattering, in LEED adsorbate and substrate are probed but the contributions of scattering centers are not clear for alaninate/Cu(110) [3,7]. The binding oxygen and nitrogen atoms, the molecular adsorption footprint, as well as substrate reconstructions were discussed [7,8,10,12]. A quantitative analysis of LEED intensities for glycine on Cu(110) showed a strong sensitivity to the position of the central carbon atom [20]. In the present interpretation of LEED and FAD data, for the alaninate phases IVa and IV via a $c(3.16 \times 2)$ unit cell, neighboring molecules alternate in their adsorption footprint, molecular modification, and, for the racemat, in their chirality. Therefore a long-range order of the lower parts of molecules is not given and they might not contribute to the LEED intensity. For the "undistorted" racemic phase IVb, triangulation measurements point to a model with the same modification of both molecules (models SR and RS) and therefore a true glide-plane symmetry is present. The LEED pattern can then be interpreted as a superposition of a $pg(3 \times 2)$ and $c(3 \times 2)$ unit cell.

VI. SUMMARY

We studied the adsorption and the atomic structure of alanine on Cu(110) by means of LEED and grazing scattering of fast atoms. Recording the specular intensity of scattered He atoms allowed us to control the adsorption process *in situ*, where a maximum indicates a coverage of one monolayer. The phase IV of enantiopure and racemic alaninate/Cu(110) with a (3×2) unit cell was investigated in detail. From the splitting of diffractions spots for fast atom diffraction (FAD), we derive the unit cell of the topmost part of the surface. We conclude that there is an arrangement of the protruding methyl groups at the corners of a $c(3 \times 2)$ unit cell based on the present FAD and triangulation studies. For the enantiopure phase IV and racemic phase IVa, the unit cell is elongated in $[1\,0]_{\mathrm{Cu}} = [\bar{1}\,1\,0]$ direction by about 5%, i.e., $c(n \times 2)$ with $n = 3.16 \pm 0.04$. This provides an explanation for the displacement of diffraction spots in LEED patterns observed in former and the present studies. The enhanced unit-cell size results in a reduced coverage $\Theta = 1/n$ for these phases. This explains the temperature-induced transition of the "undistorted" phase IVb to the "distorted" IVa by gradual desorption and the transition from IVa to IVb for dosing additional amounts of alanine. A uniformly spaced arrangement of molecules including bridge sites of the binding oxygen and nitrogen atoms seems to be unlikely, when close to on-top positions are preferred as described in literature. Also, a significant reconstruction of the substrate can be ruled out from the results of ion-beam triangulation (IBT). Instead, the binding atoms (i.e., the adsorption footprint) have local $p(3 \times 2)$ symmetry, but different deformations of neighboring molecules lead to an arrangement of methyl groups in a stretched unit cell $c(3.16 \times 2)$.

ACKNOWLEDGMENTS

This work was supported by the Deutsche Forschungsgemeinschaft under Contract No. Wi 1336. We thank K. Maass and G. Lindenberg for their assistance in the preparation of the experiments, and M. Blanco-Rey for providing the atomic positions of structural models.

[1] F. Rosei, M. Schunack, Y. Naitoh, P. Jiang, A. Gourdon, E. Laegsgaard, I. Stensgaard, C. Joachim, and F. Besenbacher, Prog. Surf. Sci. **71**, 95 (2003).
[2] F. Schreiber, J. Phys.: Condens. Matter **16**, R881 (2004).
[3] S. Barlow and R. Raval, Surf. Sci. Rep. **50**, 201 (2003).
[4] J. Williams, S. Haq, and R. Raval, Surf. Sci. **368**, 303 (1996).
[5] S. M. Barlow, S. Louafi, D. Le Roux, J. Williams, C. Muryn, S. Haq, and R. Raval, Langmuir **20**, 7171 (2004).
[6] M. Polcik, F. Allegretti, D. I. Sayago, G. Nisbet, C. L. A. Lamont, and D. P. Woodruff, Phys. Rev. Lett. **92**, 236103 (2004).
[7] S. Barlow, S. Louafi, D. Le Roux, J. Williams, C. Muryn, S. Haq, and R. Raval, Surf. Sci. **590**, 243 (2005).
[8] R. B. Rankin and D. S. Sholl, Surf. Sci. **574**, L1 (2005).
[9] R. B. Rankin and D. S. Sholl, J. Phys. Chem. B **109**, 16764 (2005).
[10] D. I. Sayago, M. Polcik, G. Nisbet, C. L. A. Lamont, and D. P. Woodruff, Surf. Sci. **590**, 76 (2005).
[11] G. Jones, L. Jones, F. Thibault-Starzyk, E. Seddon, R. Raval, S. Jenkins, and G. Held, Surf. Sci. **600**, 1924 (2006).
[12] S. Haq, A. Massey, N. Moslemzadeh, A. Robin, S. M. Barlow, and R. Raval, Langmuir **23**, 10694 (2007).
[13] W. Y. Cheong, Y. Huang, N. Dangaria, and A. J. Gellman, Langmuir **26**, 16412 (2010).
[14] M. Blanco-Rey and G. Jones, Phys. Rev. B **81**, 205428 (2010).
[15] M. Clegg, L. Morales de la Garza, S. Karakatsani, D. King, and S. Driver, Top. Catal. **54**, 1429 (2011).
[16] A. Schüller, S. Wethekam, and H. Winter, Phys. Rev. Lett. **98**, 016103 (2007).
[17] P. Rousseau, H. Khemliche, A. G. Borisov, and P. Roncin, Phys. Rev. Lett. **98**, 016104 (2007).
[18] H. Winter and A. Schüller, Prog. Surf. Sci. **86**, 169 (2011).
[19] J. Seifert, M. Busch, E. Meyer, and H. Winter, Phys. Rev. Lett. **111**, 137601 (2013).
[20] Z. V. Zheleva, T. Eralp, and G. Held, J. Phys. Chem. C **116**, 618 (2012).
[21] Sigma-Aldrich Chemie GmbH, Taufkirchen, Germany.
[22] Roentdek Handels GmbH, Germany.
[23] E. Liénard, M. Herbane, G. Ban, G. Darius, P. Delahaye, D. Durand, X. Fléchard, M. Labalme, F. Mauger, A. Mery, O. Naviliat-Cuncic, and D. Rodríguez, Nucl. Instrum. Methods Phys. Res., Sect. A **551**, 375 (2005).
[24] D. S. Gemmell, Rev. Mod. Phys. **46**, 129 (1974).
[25] H. Winter, Phys. Rep. **367**, 387 (2002).
[26] A. W. Kleyn and T. C. M. Horn, Phys. Rep. **199**, 191 (1991).
[27] A. Schüller, G. Adamov, S. Wethekam, K. Maass, A. Mertens, and H. Winter, Phys. Rev. A **69**, 050901 (2004).
[28] N. Bundaleski, H. Khemliche, P. Soulisse, and P. Roncin, Phys. Rev. Lett. **101**, 177601 (2008).
[29] A. Schüller and H. Winter, Phys. Rev. Lett. **100**, 097602 (2008).

[30] A. Schüller, M. Busch, S. Wethekam, and H. Winter, Phys. Rev. Lett. **102**, 017602 (2009).
[31] M. Busch, A. Schüller, S. Wethekam, and H. Winter, Surf. Sci. **603**, L23 (2009).
[32] A. Schüller, M. Busch, J. Seifert, S. Wethekam, H. Winter, and K. Gärtner, Phys. Rev. B **79**, 235425 (2009).
[33] J. Seifert, A. Schüller, H. Winter, R. Włodarczyk, J. Sauer, and M. Sierka, Phys. Rev. B **82**, 035436 (2010).
[34] J. Seifert, A. Schüller, H. Winter, and K. Gärtner, Nucl. Instrum. Methods Phys. Res., Sect. B **269**, 1212 (2011).
[35] A. Schüller, D. Blauth, J. Seifert, M. Busch, H. Winter, K. Gärtner, R. Włodarczyk, J. Sauer, and M. Sierka, Surf. Sci. **606**, 161 (2012).
[36] J. Seifert and H. Winter, Phys. Rev. Lett. **108**, 065503 (2012).
[37] M. Busch, J. Seifert, E. Meyer, and H. Winter, Phys. Rev. B **86**, 241402 (2012).
[38] J. Seifert and H. Winter, Surf. Sci. **610**, L1 (2013).
[39] C. A. Rios Rubiano, G. A. Bocan, M. S. Gravielle, N. Bundaleski, H. Khemliche, and P. Roncin, Phys. Rev. A **87**, 012903 (2013).
[40] A. Zugarramurdi and A. G. Borisov, Phys. Rev. A **87**, 062902 (2013).
[41] A. Zugarramurdi, M. Debiossac, P. Lunca-Popa, L. S. Alarcon, A. Momeni, H. Khemliche, P. Roncin, and A. G. Borisov, Phys. Rev. A **88**, 012904 (2013).
[42] J. Seifert and H. Winter, Nucl. Instrum. Methods Phys. Res., Sect. B **315**, 9 (2013).
[43] J. Seifert and H. Winter (to be published).
[44] R. Pfandzelter, T. Bernhard, and H. Winter, Phys. Rev. Lett. **90**, 036102 (2003).
[45] T. Bernhard, J. Seifert, and H. Winter, J. Phys.: Condens. Matter **21**, 134001 (2009).
[46] J. Seifert, D. Blauth, and H. Winter, Phys. Rev. Lett. **103**, 017601 (2009).
[47] Passivated implanted planar silicon detector (PIPS), Canberra, Inc.
[48] F. Aumayr, G. Lakits, and H. Winter, Appl. Surf. Sci. **47**, 139 (1991).
[49] We use the surface unit-cell indices $[1\,0]_{\mathrm{Cu}} = [\bar{1}10]$ and $[0\,1]_{\mathrm{Cu}} = [001]$. The substrate lattice parameters for Cu(110) are $a_1 = 2.56$ Å and $a_2 = a_{\mathrm{Cu}} = 3.615$ Å.
[50] Edited by D. R. Lide, *Handbook of Chemistry and Physics* (CRC Press, Boca Raton, FL, 2001).
[51] Y. Fujii, K. Narumi, K. Kimura, M. Mannami, T. Hashimoto, K. Ogawa, F. Ohtani, T. Yoshida, and M. Asari, Appl. Phys. Lett. **63**, 2070 (1993).
[52] R. Pfandzelter, T. Igel, M. Ostwald, and H. Winter, Appl. Surf. Sci. **142**, 470 (1999).
[53] H. Zi-Pu, D. Ogletree, M. Van Hove, and G. Somorjai, Surf. Sci. **180**, 433 (1987).
[54] Superposition of interatomic pair potentials in the Thomas-Fermi approach as proposed by D. J. O'Connor and J. P. Biersack, Nucl. Instrum. Methods Phys. Res., Sect. B **15**, 14 (1986).
[55] S. York, S. Haq, K. Kilway, J. Phillips, and F. Leibsle, Surf. Sci. **522**, 34 (2003).